U.S. ARMY COMBAT CAPABILITIES DEVELOPMENT COMMAND
CHEMICAL BIOLOGICAL CENTER

ABERDEEN PROVING GROUND, MD 21010-5424

CCDC CBC-TR-1574

Self-Constructing Kinetic Rate Equation from Experimental Rate Data Points of Heterogeneous Adsorption of Thiophenol on Gold Substrates Using Surface-Enhanced Raman Spectroscopy

Waleed Maswadeh
Richard Vanderbeek
Erik Emmons
Jason Guicheteau
Ashish Tripathi

RESEARCH AND TECHNOLOGY DIRECTORATE

May 2019

Disclaimer

The findings in this report are not to be construed as an official Department of the Army position unless so designated by other authorizing documents.

REPORT DOCUMENTATION PAGE

Form Approved
OMB No. 0704-0188

1. REPORT DATE *(DD-MM-YYYY)*	**2. REPORT TYPE**	**3. DATES COVERED** *(From - To)*
XX-05-2019	Final	Mar 2017 – Mar 2018

4. TITLE AND SUBTITLE
Self-Constructing Kinetic Rate Equation from Experimental Rate Data Points of Heterogeneous Adsorption of Thiophenol on Gold Substrates Using Surface-Enhanced Raman Spectroscopy

5a. CONTRACT NUMBER

5b. GRANT NUMBER

5c. PROGRAM ELEMENT NUMBER

6. AUTHOR(S)
Maswadeh, Waleed; Vanderbeek, Richard; Emmons, Erik; Guicheteau, Jason; and Tripathi, Ashish

5d. PROJECT NUMBER

5e. TASK NUMBER

5f. WORK UNIT NUMBER

7. PERFORMING ORGANIZATION NAME(S) AND ADDRESS(ES)
Director, CCDC CBC, ATTN: FCDD-CBR-IS, APG, MD 21010-5424

8. PERFORMING ORGANIZATION REPORT NUMBER
CCDC CBC-TR-1574

9. SPONSORING / MONITORING AGENCY NAME(S) AND ADDRESS(ES)
Defense Threat Reduction Agency, 8725 John J. Kingman Road, MSC 6201, Fort Belvoir, VA 22060-6201

10. SPONSOR/MONITOR'S ACRONYM(S)
DTRA

11. SPONSOR/MONITOR'S REPORT NUMBER(S)

12. DISTRIBUTION / AVAILABILITY STATEMENT
Approved for public release: distribution unlimited.

13. SUPPLEMENTARY NOTES
U.S. Army Combat Capabilities Development Command Chemical Biological Center (CCDC CBC) was previously known as U.S. Army Edgewood Chemical Biological Center (ECBC).

14. ABSTRACT:
Traditional practices in kinetics start with a proposed mechanism and then derive a rate model (equation), which is tested with experimental data profiles. A new approach was used to self-construct a unique, single surface-enhanced Raman spectroscopy (SERS) kinetic rate model that fits all 25 experimental rate profiles (at different temperature and pH values) without prior mechanisms, user input bias, default parameters, or rate model assumptions. The 25 experimental thiophenol (TP) adsorption data profiles on gold metal surfaces (SERS signal vs time) at four pH values and six temperatures were collected using SERS. TP adsorption rate profiles show a variety of results from a simple exponential to S-shaped rate profiles. The new SERS kinetic rate model reveals that TP adsorption has a (nearly constant) low temperature of activation ($T_a = E_a/R$ = 3000 K) at ≤pH 6. The T_a increased by 900 K to reach 3900 K under a high pH of 10. The T_a value of 3000 K was consistent with the literature for the Au–S adsorption bond. The increase in T_a by 900 K (i.e., 3000 to 3900 K) was consistent with the difference due to pH changes corresponding to the protonation state.

15. SUBJECT TERMS
Self-constructing kinetic rate model (SCRM) | Kinetic modeling | Kinetic dataset fitting
Surface-enhanced Raman spectroscopy (SERS) | Biosensor | Heterogeneous adsorption

16. SECURITY CLASSIFICATION OF:			**17. LIMITATION OF ABSTRACT**	**18. NUMBER OF PAGES**	**19a. NAME OF RESPONSIBLE PERSON**
a. REPORT	**b. ABSTRACT**	**c. THIS PAGE**			Renu B. Rastogi
U	U	U	UU	36	**19b. TELEPHONE NUMBER** *(include area code)* (410) 436-7545

Blank

PREFACE

The work described in this report was started in March 2017 and completed in March 2018. At the time this work was performed, the U.S. Army Combat Capabilities Development Command Chemical Biological Center (CCDC CBC) was known as the U.S. Army Edgewood Chemical Biological Center (ECBC).

The use of either trade or manufacturers' names in this report does not constitute an official endorsement of any commercial products. This report may not be cited for purposes of advertisement.

This report has been approved for public release.

Acknowledgments

The authors acknowledge Dr. A. Peter Snyder (retired ECBC) for his technical discussions, editing, and guidance.

Blank

CONTENTS

FIGURES

TABLES

SELF-CONSTRUCTING KINETIC RATE EQUATION FROM EXPERIMENTAL RATE DATA POINTS OF HETEROGENEOUS ADSORPTION OF THIOPHENOL ON GOLD SUBSTRATES USING SURFACE-ENHANCED RAMAN SPECTROSCOPY

1. INTRODUCTION

Kinetic equations in the literature are used in an attempt to fit experimental rate profiles (intensity or concentration vs time) with a number of rate models. If a reasonable fit to a rate model is observed, then the mechanism(s) involved in that rate model will be used, by default, to explain the experimental data. For example, Ho and McKay found kinetic rate models in the literature that best fit the absorption of copper ions by peat. They tried a number of traditional rate models and concluded that because of the high correlation coefficients obtained using the Elovich and pseudo-second-order models, the absorption of copper ions by peat followed a first-order kinetic model (*1*). But they did not determine which sorption mechanism actually occurred or what mechanism was responsible for the ability of peat to sorb copper ions.

If no traditional rate models in the literature provide a satisfactory fit with experimental data, then efforts are directed toward creating mechanisms that are followed by rate equations to interpret experimental data. This approach (creating mechanisms and rate equations) led many to devise kinetic rate models that consist of multiple fitting parameters suitable for a wide variety of rate profiles (overfitting).

Time-, temperature-, and pH-dependent signal intensity measurements of thiophenol (benzenethiol) adsorption on commercial nanostructured gold substrates are probed using surface-enhanced Raman spectroscopy (SERS). SERS is a highly sensitive characterization technique discovered in the 1970s by Fleischmann et al. (*2*). Many of the molecules reported in SERS experiments are generally restricted to classes of molecules that tend to strongly bind at the nanostructured substrate surface (e.g., thiols, amines, and aromatic macrocycles) (*3*). Seelenbinder et al. (*4*) showed that SERS works only for polar molecules that have electron-withdrawing character. However, less polar, aliphatic-substituted heterocyclic and polycyclic aromatics bind more strongly on gold as compared with thiophenol. In the Seelenbinder study, some analytes, although they did not strongly bind to gold, were placed onto the self-assembled monolayers of thiophenol on gold substrate, and SERS spectra were obtained. SERS enhancement was accomplished using analytes that were not bound to the metal surface (gold).

A gray area exists between physisorption and chemisorption with respect to activation energy. The general rule is that physisorption is the process where the structure of a molecule does not change or alter when it adheres to the surface; whereas chemisorption is a process in which the structure of a molecule does alter when it adheres to the surface. Thiophenol binds to a gold surface due to the strong affinity of the –SH group to gold. Thiols are generally chemisorbed on noble metals through the loss of the sulfhydryl hydrogen, and a bond forms between the thiol sulfur and the metal surface (*5*–*7*). Adsorption characterization of thiophenol (kinetics, energetics, and reaction mechanisms) is not fully understood, although several groups have studied the adsorption of thiophenol on metallic surfaces. Love et al. (*5*) stated that the fate of hydrogen in the S–H groups had not been determined unambiguously. In vacuum studies, hydrogen loss is in the form of dihydrogen or the reductive elimination of H_2

from Au^{3+}, and is a weakly activated process. Nara et al. (*8*) stated that thiophenol dissociated into thiolate molecules and H atoms, and both were adsorbed on the gold surface. The adsorbed H atoms are desorbed in the gas or liquid phase as hydrogen molecules. Dumee et al. (*9*) showed that the hydrogen adsorption energy from gold nanoparticles plated on carbon nanotube substrates was approximately 810 kJ/mol.

The activation energy for the S–H bond was measured by Dubois et al. (*10*) for the chemisorption of ethanethiol and methanethiol from the gas phase onto a gold substrate and found to be in the range of 21–29 kJ/mol. It was hypothesized that this activation energy is required for organothiol dissociative attachment (R–SH + Au to R–S–Au + ½H_2). Further evidence of a dissociative attachment mechanism is shown by the disappearance of the S–H in-plane-bending vibrational mode, located at 918 cm^{-1} (*11*). Nuzzo et al. (*12*) estimated the barrier to chemisorption of methanethiol from the gas phase as 25 kJ/mol. Wetterer (*13*) stated that the physisorption energy contributed by the thiol group is on the order of 33 kJ/mol, whereas the sulfur atom alone contributes ~24 kJ/mol.

1.1 Standard or Traditional Approach

Researchers tend to focus on developing a mechanism before acquiring rate profiles. Efforts consist of devising mechanisms, developing an experimental setup, and then devising and testing kinetic rate model(s). The kinetic rate model may closely track the experimental data points. The traditional steps involved are (1) collecting experimental rate profiles, (2) developing a mechanism, (3) developing the rate model from step 2, (4) testing the rate model from step 3, and (5) repeating steps 2–4, if step 4 is unsuccessful. Other traditional steps involved are (1) collecting experimental rate profiles, (2) testing the traditional rate model(s) found in the literature, (3) selecting traditional rate model that produce high degrees of correlations with the experimental data, and (4) developing a mechanism from step 3 that can explain the chosen rate models.

Before trying to gain a fundamental understanding of the reaction mechanisms and kinetics of binding a molecule on non-functionalized gold SERS substrates, the proper rate profiles and models should be accurately measured and constructed, respectively. Multiple rate profile measurements were made to accomplish this.

Thiophenol is one of the most studied SERS-active molecules because the strong affinity of thiols to gold or noble metal surfaces produces strong SERS spectra (*14–17*). Such information can help explain some of the findings and calculated parameters in this study. A variety of substituted thiols have been examined for the pH dependence of their adsorption properties and SERS responses (*18–20*). These literature studies (*18–21*) focused on the bonding state between the surface and analyte. Efforts herein attempt to explain the mechanisms involved in this bonding. The adsorption mechanism is expected to depend on the physical state of the material, as well as the environment that surrounds the thiophenol molecule and the surface.

1.2 New Self-Constructing Model Approach

For this study, a single rate model was created in which only the experimental rate data points were used to build a kinetic rate model without prior mechanisms, user-input bias, or default-fitting parameter values and assumptions. In addition, the mechanisms of thiophenol binding on gold surfaces, as a function of pH and temperature, are proposed from a self-constructed rate model.

The self-constructed model approach also has constants as part of the derivation. These constants have an actual meaning that are characteristic of the analyte and experimental variables.

The new, suggested approach consists of the following: (1) collecting experimental rate profiles, (2) creating the kinetic rate model from step 1, and (3) suggesting a mechanism(s) that produces the rate model from step 2.

2. MATERIALS AND METHODS

Detailed sample preparations, gold SERS substrates, Raman microscopy, temperature control, and sample-handling for this type of study have been presented by Tripathi et al. (*22*).

2.1 Sample Preparations

Thiophenol (benzenethiol) was purchased from Sigma-Aldrich (catalog no. 20249-10G; St. Louis, MO), and stock solutions were prepared in ethanol at various concentrations and then diluted to final working concentrations with deionized water (18.2 MΩ·cm). Hydrochloric acid (Sigma-Aldrich catalog no. 320331-2.5L) and sodium hydroxide (Sigma-Aldrich catalog no. 221465-25G) were used to obtain low and high pH values, respectively. A 35 μL volume of stock thiophenol solution in ethanol (with different concentrations) was added to 7 mL of aqueous medium (with a selected pH value), to yield an ethanol content of 0.5%. The final solution was vigorously shaken and equilibrated for at least 30 min at the same temperature as the gold substrate.

2.2 Gold SERS Substrate

Commercially available gold SERS substrates (Klarite, KLA-312; Renishaw Diagnostics Limited; Glasgow, U.K.) were used and are shown in Figure 1, which was obtained using a scanning-electron microscope (SEM; Pro-X desktop model; Phenom World; Eindhoven, The Netherlands). The plasmon reflectivity spectrum (model QR450-7-XSR; Ocean Optics; Dunedin, FL) of a typical Klarite substrate is shown in Figure 1. Stationary planar SERS substrates offer an advantage over colloidal substrates for kinetics studies, as noted by Tripathi et al. (*22*).

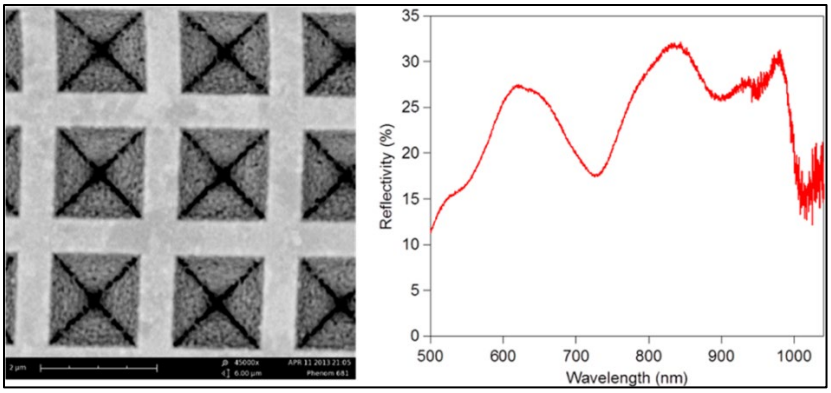

Figure 1. SEM image (left) and plasmon reflectivity spectrum (right) of a Klarite substrate.

2.3 Raman Microscopy

The Raman measurements were performed with a NRS-3200 dispersive Raman microscope system (Jasco Analytical Instruments; Easton, MD) operating at 785 nm excitation with approximately 4 mW of power incident on the sample. A 10× microscope objective was used to focus the laser on the substrate and to collect the Raman scattered light. The Raman scattered light was dispersed with a 600 grooves/mm diffraction grating, and a spectrometer entrance slit width of 100 µm was used to obtain a spectral resolution of approximately 8 cm^{-1}. The Raman scattered light was detected with a thermoelectrically cooled charge-coupled device or CCD camera (Andor Technology, Oxford Instruments; Belfast, Ireland). The strong Rayleigh scattered light was suppressed with a notch filter (Semrock, IDEX Health and Science; Rochester, NY).

2.4 Temperature Control and Sample Handling

A temperature-controlled analyte sample chamber (ASC) system was designed, as shown in Figure 2, to maintain isothermal conditions for the 7 mL of thiophenol solution and gold Klarite substrate. The ASC was composed of a Klarite substrate mounted in a 50 mm diameter polystyrene Petri dish (model 351006; BD Biosciences; Franklin Lakes, NJ), a magnetic stir bar (catalog no. 1451363; Fisher Scientific; Pittsburgh, PA), and a 3 mm diameter hole in the lid of the Petri dish, covered by a thin quartz slide to prevent any evaporation. The ASC sample holder was temperature-controlled by placing it in thermal contact with a liquid-cooled copper block that had a water/ethylene glycol mixture circulating through it. The temperature of this mixture was regulated by a closed-loop refrigeration/heating system (model MX 07R-20A11B; PolyScience; Niles, IL). New gold Klarite substrates and polystyrene Petri dishes were used for each experiment.

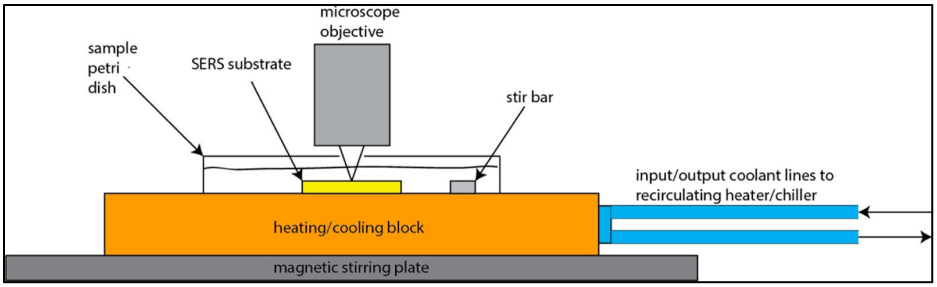

Figure 2. Schematic diagram of the temperature-controlled SERS setup.

2.5 Experimental Rate Profiles

Experimental thiophenol rate profiles (SERS signal vs time) at pH 2, 4, 6, and 10 and at six different temperatures, for a total of 25 rate profiles, were acquired using commercial nanostructured gold substrates for SERS investigations. Thiophenol was chosen because of the strong affinity of the –SH group to gold metal.

3. RESULTS AND DISCUSSION

The focus of this study was to create a kinetic rate model by using only the experimental rate data points at different temperature and pH values without any prior selection of traditional rate models that are found in the literature or without the development of mechanisms, user bias, or assumptions. This approach was called self-constructing rate modeling (SCRM).

Some of the experimental rate profile measurements for the SCRM were collected at low temperatures and low pH to ensure that some rate profiles were close to the rate-limiting step (e.g., diffusion). At low temperatures, the diffusion rate step becomes slower, and this leads to diffusion-limited rates (*23*). A detailed discussion of the experimental setup and approach (including the optimal concentration of thiophenol to be used) to produce experimental rate profiles can be found in Tripathi et al. (*22*). The reported acid dissociation constant (pK_a) for thiophenol at room temperature is in the range of 6.5−8.0 (*24–27*).

Examples of SERS rate profiles for thiophenol interaction with gold Klarite substrate at various pH values and temperatures are shown in Figure 3. In each case, 7 mL of 5×10^{-7} M thiophenol solution in aqueous media was added to the sample chamber, and the Raman spectral response was recorded as a function of time.

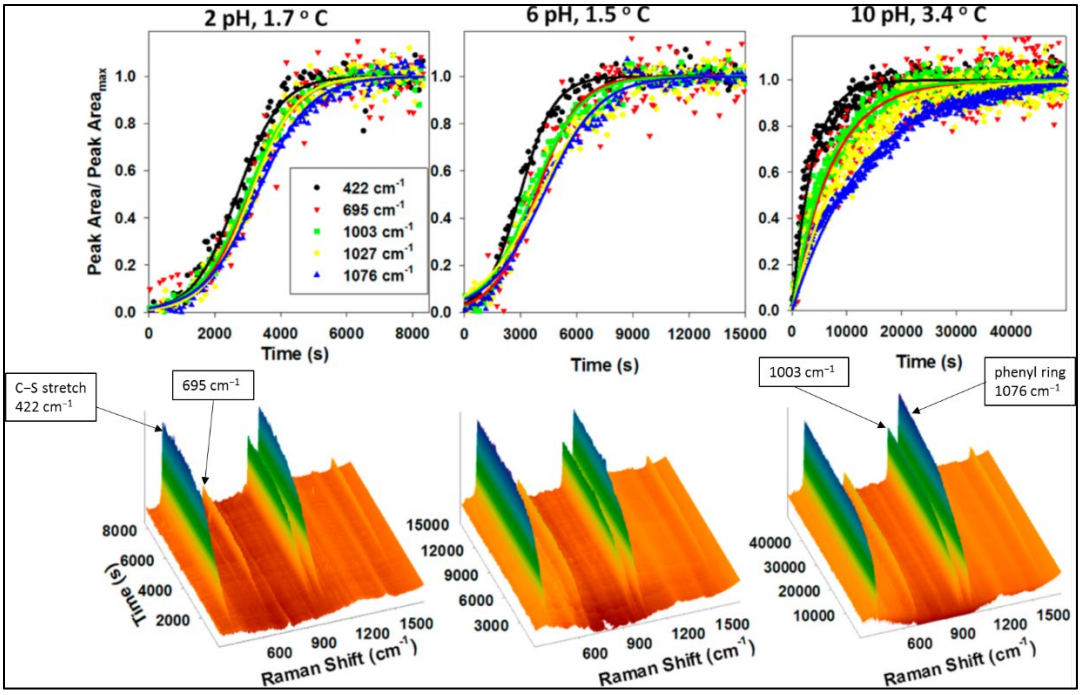

Figure 3. SERS rate profiles for thiophenol with gold Klarite substrate at selected pH and temperatures.

Figure 3 shows SERS rate profiles for pH 2, 6, and 10 at constant temperatures of 1.7, 1.5, and 3.4 °C, respectively. The top panels in Figure 3 display scaled temporal signal responses of a few selected Raman-active vibrations for the thiophenol molecule at 422, 695, 1003, 1027, and 1076 cm^{-1}. The bottom panels in Figure 3 show the Raman spectral responses in three-dimensional (3D) displays (Raman shift, time, and intensity). The 3D display indicates that the overall rate of thiophenol adsorption decreases as the pH values decrease or the temperature of activation ($T_a = E_a/R$; where E_a is the activation energy and R is the universal gas constant) decreases. It was observed that in acidic solution (pH 2), there is a significant delay in time before the Raman spectral features begin to increase. The scaling was done by dividing the peak area at a given time by the maximum peak area (saturation value) for each Raman-active vibration of the thiophenol molecule (422, 695, 1003, 1027, and 1076 cm^{-1}).

It is clear from Figure 3 that the thiophenol rate profile for the 422 cm^{-1} band (black curve) reaches the saturation point faster than that of the four other vibrational band profiles. A similar phenomenon was observed by Biggs et al. and was attributed to a change in the angle of the C−S stretch (*14*). The phenyl ring mode at 1076 cm^{-1} shows the strongest band intensity (Au–S bond) when compared with the remaining Raman features and is primarily used in collecting experimental rate profiles.

Figure 4 shows normalized experimental rate profiles for thiophenol, acquired at different pH and temperature values. Normalization or relative intensity (Ri) was calculated using

$$\mathrm{Ri} = \mathrm{Ri}_{max}\,(I - I_{min})/(I_{min} - I_{max}) \qquad (1)$$

where I is the SERS intensity (variable at 1076 cm^{-1}), I_{min} is the minimum SERS intensity (normally zero), I_{max} is the maximum SERS intensity, and Ri_{max} is a fitting parameter from 0.90–1.0. An Ri_{max} value of less than 1.0 was chosen, if the collected data did not reach saturation or equilibrium.

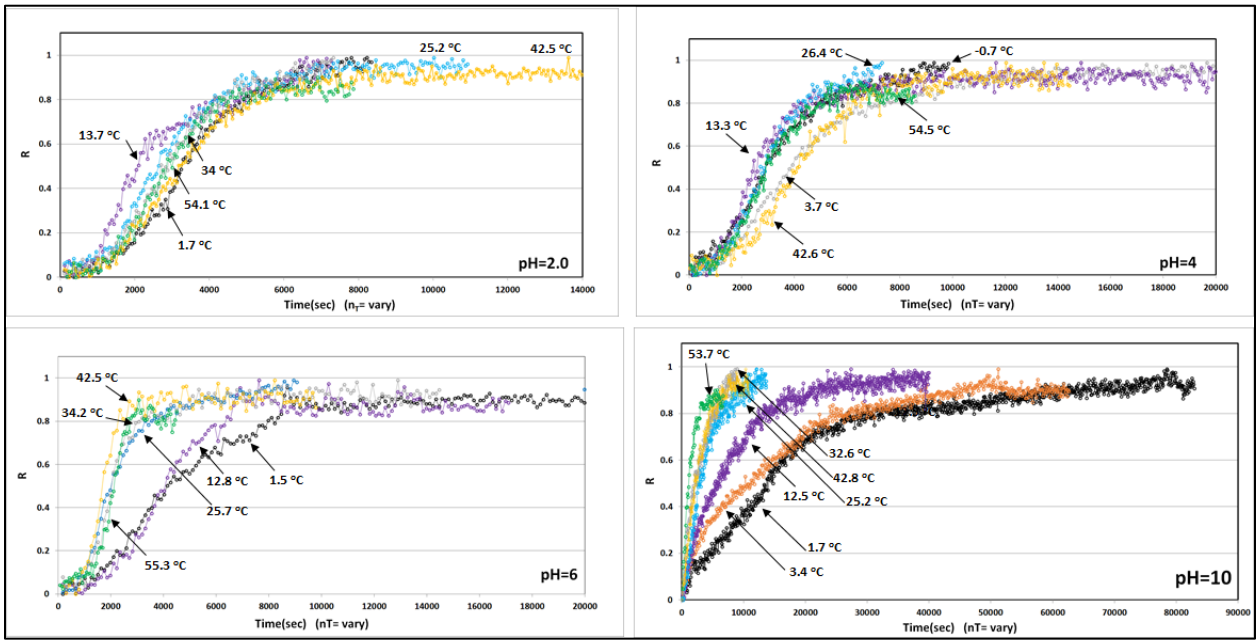

Figure 4. Normalized experimental rate profiles for thiophenol at different pH and temperature values.

The rate profiles for thiophenol at pH 10 (Figure 4, bottom right) show more temperature dependency than that of the other pH values. Profiles for thiophenol at pH 2 (Figure 4, top left) show the least temperature dependence, and the profile at 13.7 °C did not follow the general trend of the other profiles. The rate profiles for thiophenol at pH 6 (Figure 4, bottom left) show strong temperature dependences at 12.8 and 1.5 °C. The rate profiles for thiophenol at pH 4 (Figure 4, top right), in particular those at 42.6 and 3.7 °C, show a temperature dependence. These aberrant observations cannot be explained by the rate models that are available in literature. These aberrant observations are discussed and further explained herein.

Figure 5 shows a new method for normalizing the experimental rate profiles for thiophenol in both the x and y axes, as presented by Maswadeh et al. (*28*). This presentation of experimental profiles is more useful than the traditional format of time versus intensity or time versus Ri (eq 1). The new format in Figure 5 is temperature, time, and intensity independent (dimensionless or relative). Figure 5 shows clearly that at each pH value, all experimental profiles at different temperatures share similar overall mechanisms with respect to the common slope of the curves. The overall mechanism changes with changing pH. Rate profiles are sigmoidal at low pH values and then change to an exponential shape (first-order) from pH 6 to 10.

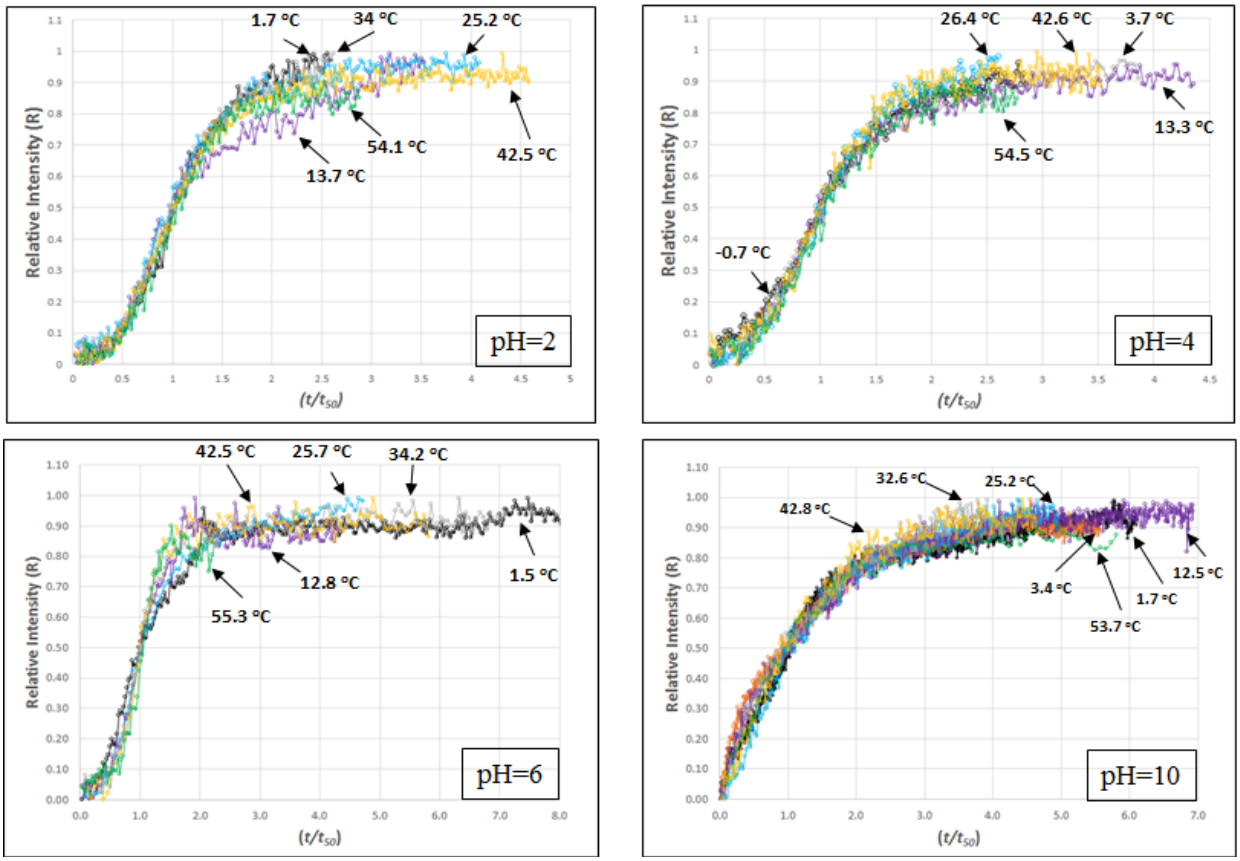

Figure 5. Normalization of the experimental profiles for thiophenol at pH 2, 4, 6, and 10 and temperatures in both axes (Maswadeh et al. [*28*]). This format is convenient to present the experimental profiles compared with the traditional format of time versus intensity or time versus Ri.

3.1 Self-Constructing Kinetic Rate Model

A new approach (to be documented in a later report) was constructed by studying various traditional kinetic rate models with one and two rate constants, as found in the literature. The new approach has the ability to construct a kinetic rate equation using only experimental rate data points with no user bias, no assumptions, no default parameter values, and no mechanism developments or modifications of any available literature rate models (equations). The new approach used all data points of the 25 experimental profiles for thiophenol at varying temperature and pH values. The following rate model equation was self-constructed:

$$\ln(1 - R) = -A \exp[-m\, T_a/T]\, (t)^m \qquad (2a)$$

where A is the Arrhenius constant, T_a is activation temperature in Kelvin, T is temperature, t is time, and m is a ratio

$$m = (1 - T/T_0)/\,(1 - T/T_e) \qquad (2b)$$

where T_0 is the temperature of immobility of analyte, and T_e is the temperature of the system at equilibrium and pH = 0. T_a, T_0, and T_e are constants (Table 1) and were calculated through self-constructed eqs 2a and b. For each pH value, there is a single value or characteristic temperature constant for T_a, T_0, and T_e.

Table 1. Calculated T_a, T_0, and T_e Values (Kelvin) at each pH from the Experimental Rate Profiles for Thiophenol

pH	$T_a = E_a/R$	T_0	T_e
2	2985	104.8	183
4	3052	126.3	203
6	3002	173.2	228
10	3870	184	293

Note: The values of T_0 and T_e increase as pH increases.

3.2 Explanations of the Three Temperature Constants (T_a, T_0, and T_e)

3.2.1 T_a: Temperature of Activation

T_a is calculated ($T_a = E_a/R$) in degrees Kelvin. Figure 6 shows a plot of pH versus calculated $T_a = E_a/R$ from Table 1. A linear relationship was not found. E_a is the minimum quantity of energy that the thiophenol species must possess in order to undergo adsorption onto gold Klarite substrate. Adsorption is complex and is a process of adhesion of thiophenol molecules onto a solid gold surface. This process creates a film of thiophenol adsorbate. An ideal surface will produce a single T_a, and in practice, a surface will produce an average T_a value. For thiophenol to adhere onto the gold surface, the chemisorption process noted by Li et al. (*11*) is involved. It was hypothesized that this activation energy is required for organothiol dissociative attachment (RSH + Au to RS--Au + ½H_2; [--] indicates an adsorption bond). Further evidence of a dissociative attachment mechanism is in the disappearance of the S–H in-plane-bending vibrational mode located at 918 cm^{-1}.

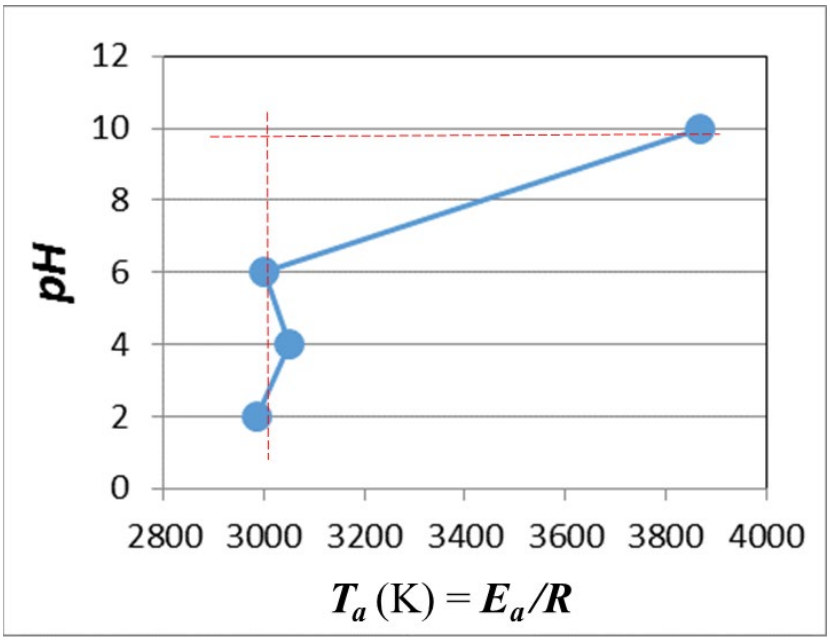

Figure 6. Plot of pH vs T_a that shows nonlinearity for thiophenol data from Table 1.

The activation energy, E_a, was measured by Dubois et al. for the chemisorption of ethanethiol and methanethiol gas on gold substrate and was found to be in the range of E_a = 21–29 kJ/mol (T_a = 2530–3494) (*10*). A study by Wetterer (*13*) indicated that the E_a contributed by a thiol group was on the order of 33 kJ/mol (T_a = 3976), whereas the sulfur atom alone contributed ~24 kJ/mol (T_a = 2892). According to Wetterer's study, the difference in E_a was 9 kJ/mol (T_a = 1084) (*13*). The newly constructed kinetic rate model discussed herein showed that thiophenol adsorption had a nearly constant activation energy at pH 6 and below (Figure 6). The T_a increased by 900 K (7.5 kJ/mol) at pH 10 and was close to Wetterer's finding. The T_a in Table 1 was approximately 3000 K for thiophenol rate profiles at pH 6 and below. This was similar to that of Dubois et al. (*12*) (E_a/R = 2530–3494 K) and of Wetterer et al. (*13*) (E_a/R = 2892 K).

As the environment of the SERS becomes more acidic in nature (pH < 7), the primary process is chemisorption (dissociation) with a nearly constant activation energy. As the environment of the SERS becomes more basic (pH > 7), the primary process is still chemisorption but at a higher T_a by 900 K, as was also indicated by Wetterer (*13*). The chemisorption mechanisms changed due to the pH environment, and the T_a increased from 3000 to 3900 K. Switching from an acidic to an alkaline environment was responsible for the chemisorption T_a increase by 900 K. That increase was most likely due to the two reaction paths from acidic to basic pH.

The two reaction paths can shed light on the difference between the two calculated temperatures of activation constants (900 K). Thiophenol at room temperature has a pK_a value in the range of 6.5−8.0 (*24–27*, *29*). This can be described as follows:

1. At pH 7, thiophenol contained 50% non-ionized thiophenol molecules (TP_{-S-H}) in equilibrium with 50% ionized thiophenolate (TP_{-S^-}).
2. At pH < 6.5, (TP_{-S-H}) contained 100% thiophenol molecules (TP_{-S-H}), no ionization.
3. At pH > 8, (TP_{-S-H}) was ionized to 100% thiophenolate (TP_{-S^-}).

The two reaction paths are

Acidic: for pH < 6.5

$$(TP_{-S-H}) + Au \rightarrow (TP_{-S^-})\text{--}Au + Au\text{--}H \quad (4)$$

Alkaline: for pH > 8.0

$$(TP_{-S^-}) + Au \rightarrow (TP_{-S^-})\text{--}Au \quad (5)$$

The notation (--) indicates an adsorption bond. The difference in activation temperature (900 K) was most likely due to the Au--H adsorption energy. Lanin et al. (*30*) calculated adsorption energies using density function theory, with a non-empirical local PBE (Perdew, Burke, and Ernzerhow) function between the gold and hydrogen atoms [R(Au--H)] of C_1–C_8 alkanes with different structures at locations of a Au_{20} cluster. Those energies were in the range of 3–14 kJ/mol (an average of E_a = 8.5 kJ/mol or T_a =1024 K). This showed that the adsorption energy of the Au--H bond aided in the reduction of the T_a in an acidic environment by 1024 K, which was very close to the experimental value of 900 K.

Holze (*31*) concluded from his study of thiophenol interactions with gold surface, TP_{-S}--Au, that the aromatic ring of thiophenol is directed away from the gold surface in aqueous solutions of 1 M $HClO_4$ (Acros Organics; Geel, Belgium) and 0.1 M $KClO_4$ (Merck and Company; Kenilworth, NJ) at pH = 4.90, unbuffered. The dominant driving force of adsorption is the Au–S bond energy.

3.2.2 T_0: Temperature of Immobility of Analyte

T_0 represents the highest temperature at which the ionic and molecular mobility (diffusion process) are frozen (T_{freeze}) or immobile, and thiophenol or thiophenolate cannot move toward the gold SERS surface to adsorb, even at infinite time. As the mobility of ions and molecules in a solution at room temperature (T_{room}) increases (e.g., by pH difference), the temperature difference ($T_{room} - T_{freeze}$) required to immobilize the ions and molecules ($T_{immobilization}$) increases so that $T_{freeze} = T_{immobilization}$. The calculated T_0 is equivalent to $T_{immobilization}$. The mobility of thiophenol in aqueous solution is therefore directly proportional to the temperature difference ($T_{298} - T_0$).

Figure 7 shows a plot of pH versus $T_{298} - T_0$, which demonstrates that there is an approximately linear relationship between $T_{298} - T_0$ and pH. As the pH increased from 1 to 7, there was a nearly linear decrease in average mobility for thiophenol in aqueous solution, as shown in Figure 7. But the mobility of thiophenol in aqueous solution stayed approximately constant for a pH near 7 or higher. This mobility versus pH behavior has been cited by many scientists (*32*–*33*).

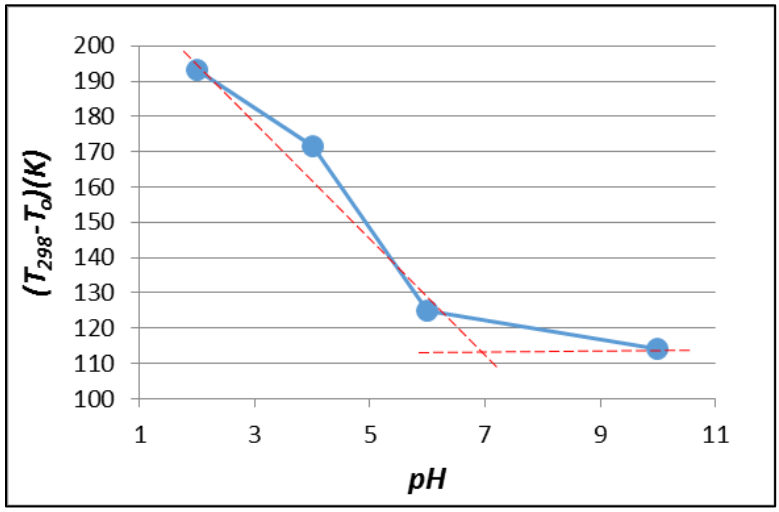

Figure 7. Plot of pH vs temperature difference ($T_{298} - T_0$).

Aider et al. (*32*) and Sánchez-Moreno et al. (*33*) have produced similar plots of pH versus mobility. Aider et al. (*32*) presented findings of behavior similar to that shown in Figure 7 for the electrophoretic mobility of mixtures of chitosan oligomers at a concentration of 0.03 to 0.003% in water at pH 2–12. Sánchez-Moreno et al. (*33*) also described the behavior of pH versus mobility for the electrophoretic mobility of lipid nanocapsules with a variety of phospholipid shells (e.g., phosphatidylserine, lecithin, Pluronic F68 surfactant [Thermo Fisher Scientific, Inc.; Waltham, MA], or chitosan) in aqueous solution at pH 4–9 as being similar to the plot shown in Figure 7.

3.2.3 T_e: Temperature of the System at Equilibrium

The value of T_0 is smaller than the value of its respective T_e value (Table 1), and the ratio T_0:T_e is approximately 10:15.

pH is defined as the negative base 10 logarithm of the hydrogen ion concentration ($pH = -\log_{10}[H^+]$). The natural logarithm form is $\ln[H^+] = -2.3\log_{10}[H^+]$.

Figure 8 shows a plot of $1/T_e$ versus pH for thiophenol on gold substrate. There is a linear relationship between $1/T_e$ and pH. T_e intersects the *x* axis at 168 K when the pH = 0. The negative slope indicates that the thiophenol adsorption process was endothermic, and the linear profile suggested an equilibrium system. This can be understood and explained by examining a pure water system.

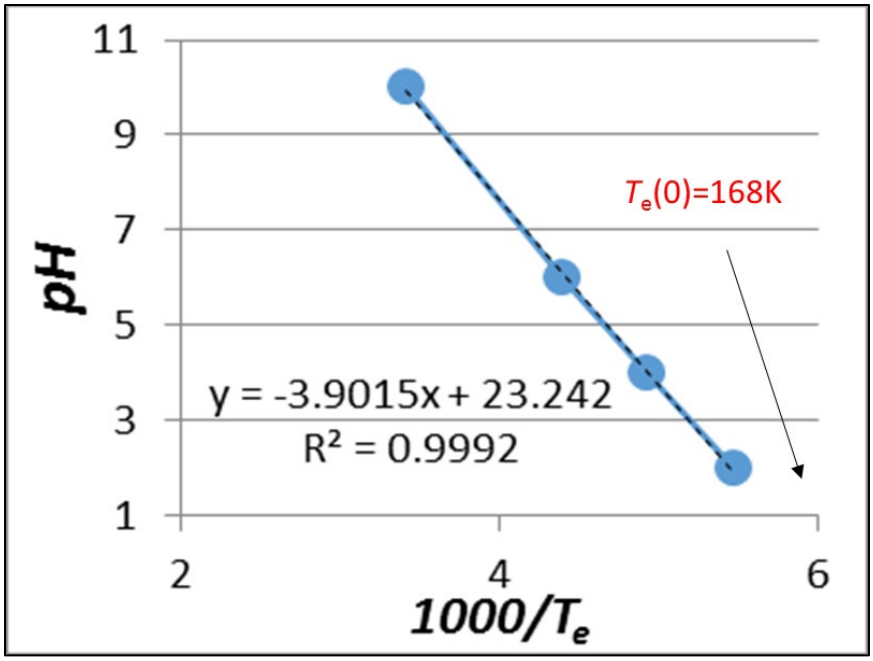

Figure 8. Plot of $1/T_e$ vs pH from Table 1. There is a linear relationship between $1/T_e$ and pH. The T_e value that intersects the *x* axis is 168 K where pH = 0.

A water (aqueous) system is always at equilibrium as

$$2H_2O \rightleftharpoons H_3O^+(aq) + OH^-(aq) \quad (6)$$

Adding reactant or altering the temperature shifts the water system until it reaches equilibrium again. The reaction is exothermic, which means that increasing the water temperature (T_{water}) decreases the pH (Table 2), as listed by Light (*34*). This occurs because the reaction shifts to the left or to the lower concentration of hydrogen ions. Likewise, decreasing the water temperature increases the pH. Table 2 lists pure water pH values at different temperatures.

Table 2. Pure Water pH Values at Different Temperatures

Property	**Condition**							
T_{water} (°C)	0	10	20	25	30	40	50	100
T_{water} (K)	273	283	293	298	303	313	323	373
pH	7.47	7.27	7.08	7	6.92	6.77	6.64	6.14

Figure 9 shows a plot of pH versus $1/T_{water}$ for pure water from Table 2. There is a linear relationship between $1/T_{water}$ and the pH of water. The slope in Figure 9 indicates the reaction type, either exo- (positive slope) or endo-(negative slope) thermic reaction. Standard notation is that as the pH decreases, the $[H^+]$ ion concentration increases. Table 2 shows that as the water temperature increases, the mobility of ions and molecules increases, the pH decreases, and the $[H^+]$ increases. The pH values ranged from 0 to 14. There are two intersections in

Figure 9, the first intersection is at pH = 0 (x axis), and the second intersection is at pH = 14 (x axis in Figure 10), corresponding to –546 and 117 K, respectively. Table 2 shows that the minimum pH value is 6.14 for water at boiling point or 373 K and cannot reach pH 0, whereas the pH of water will reach the value of 14 when the temperature is lowered to 117 K.

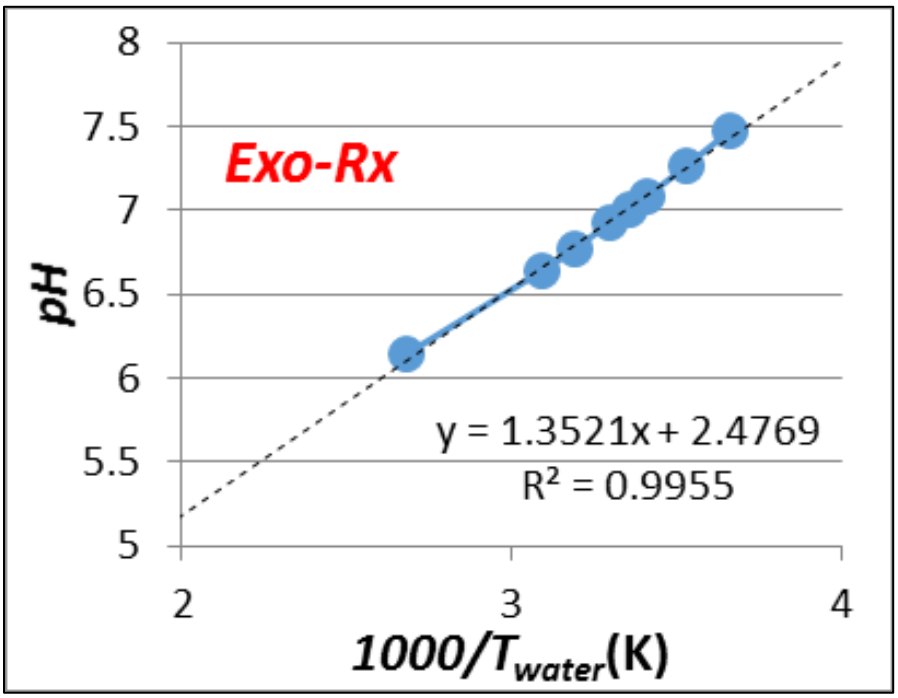

Figure 9. Plot of pure water pH vs $1/T_{water}$ from Table 2. A linear relationship between $1/T_{water}$ and pH is shown. Exo-Rx is exothermic reaction.

Figure 10 shows an indirect plot for pure water $[H^+]$ using pH versus $1/T_{water}$. There is a linear relationship between $1/T_{water}$ and pH 14. The straight line intersected the x axis at approximately 117 K, and the $[H^+]$ was close to zero. This suggests that the mobility of ions and molecules was reduced to zero or a frozen state (immobilization) at 117K.

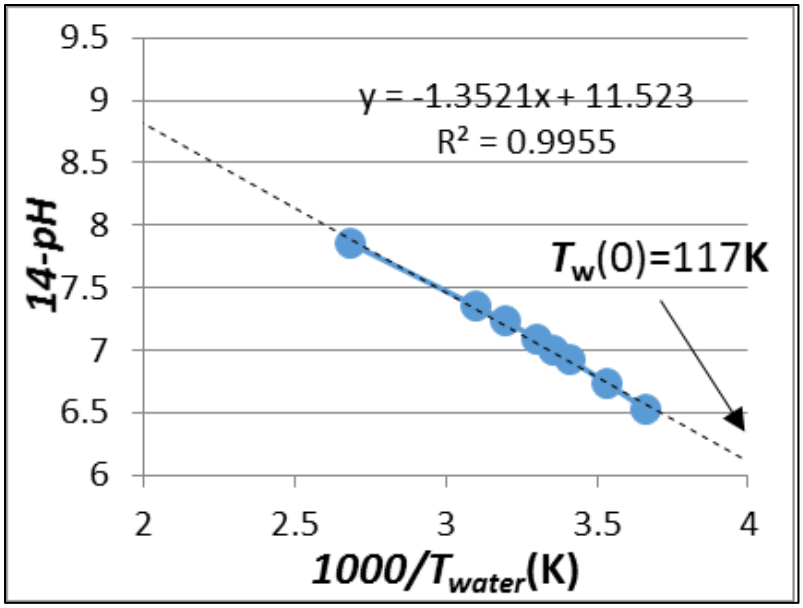

Figure 10. Plot of 14-pH vs $1/T_{water}$ for pure water. There is a linear relationship between $1/T_{water}$ and 14-pH.

Reducing the pH (or increasing 14-pH) and/or increasing the temperature in aqueous solution increases the mobility of ions and molecules. To keep the mobility constant in an aqueous solution consisting of ions and molecules, the temperature needs to be decreased as the pH value decreases. This phenomenon explains why T_e and T_0 tend to decrease as the pH decreases (Table 1). To keep the ions and molecules in a frozen state (close to zero mobility), the immobilization temperature T_0 value was found to be 105, 126, 173, and 184 K for pH values of 2, 4, 6, and 10, respectively (Table 1).

3.3 Experimental Rate Profiles and the Self-Constructed Kinetic Rate Equation: Application and Prediction

Figures 11–14 show the plots obtained by applying the new kinetic rate model (eq 2) over all 25 experimental rate profiles at different temperature and pH values.
Figure 11 shows the experimental (jagged) rate profiles (time vs Ri) at pH 2. The smooth lines were obtained using eq 2, with T_0 = 104.8 K, T_e = 183 K, T_a = 3000 K, and A = 99. The calculated T_a changed slightly, from 2800 to 3200 K, as the SERS temperature increased from 1.7 to 54.1 °C. This was within the range observed by Dubois et al. (*10*).

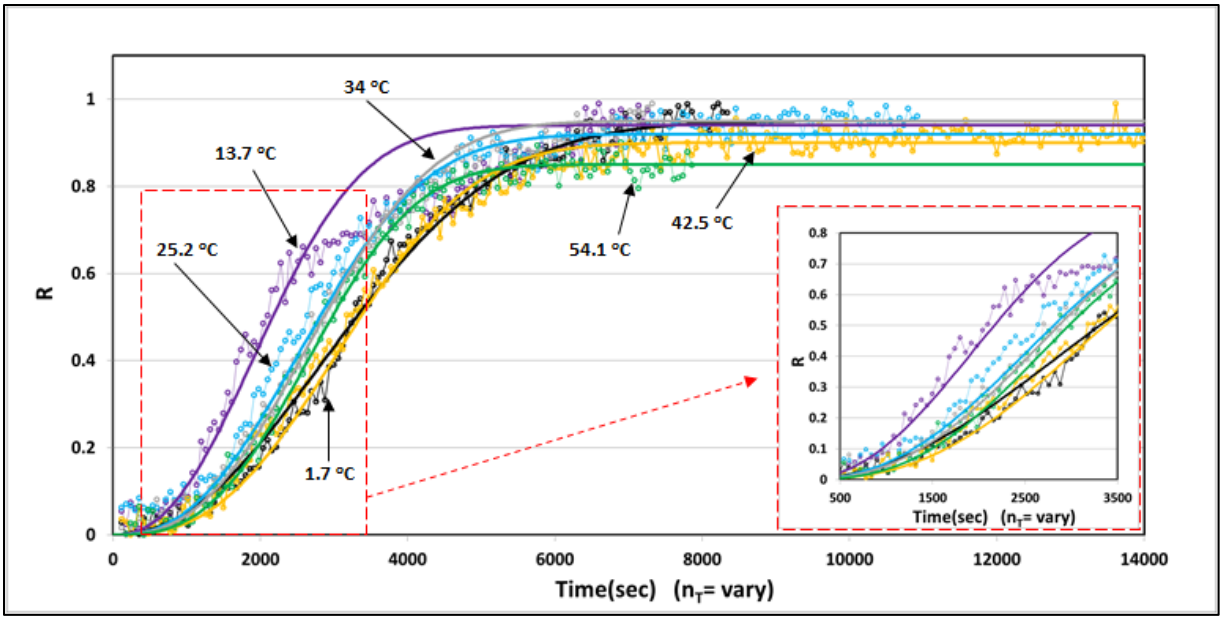

Figure 11. Experimental (jagged) rate profiles (time vs Ri) at pH 2. Smooth lines were obtained using eq 2, with T_a = 2985 K, T_0 = 104.8 K, T_e = 183 K, and A = 99.

Figure 12 shows experimental (jagged) rate profiles (time vs Ri) at pH 4. The smooth lines were obtained by using eq 2, with T_0 = 126.3 K, T_e = 203 K, T_a = 3052 K, and A = 99. The calculated T_a value also changed from 2900 to 3200 K, as the SERS temperature increased from –0.7 to 54.5 °C, but this was within the range observed by Dubois et al. (*10*).

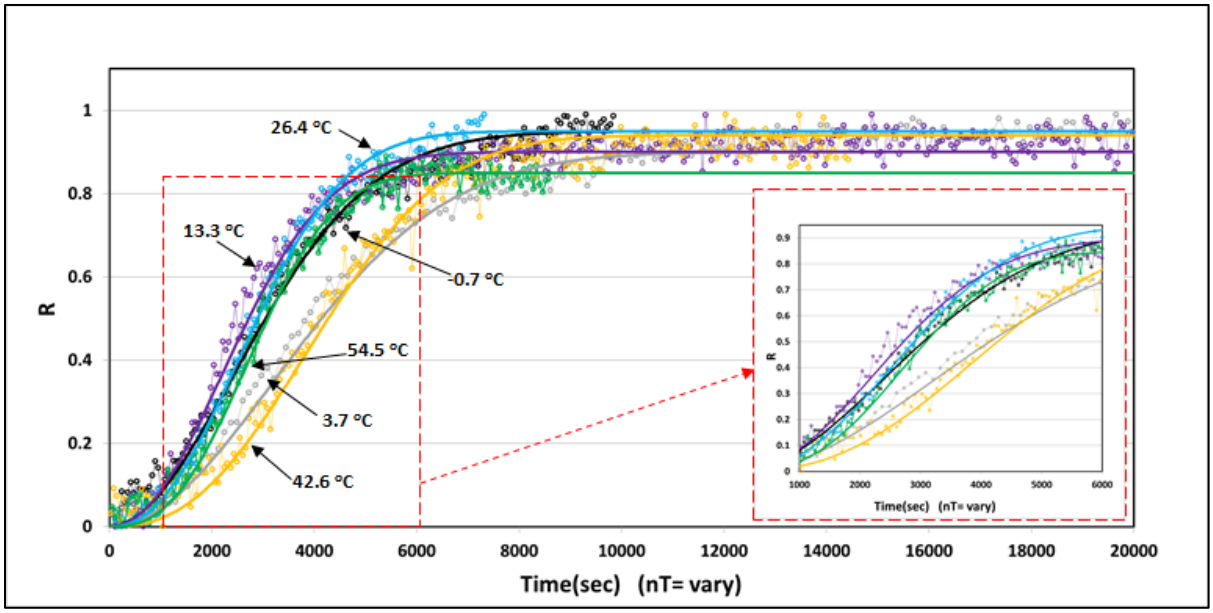

Figure 12. Experimental (jagged) rate profiles (time vs Ri) at pH 4. Smooth lines were obtained using eq 2 with T_a = 3052 K, T_0 = 126.3 K, T_e = 203 K, and A = 99.

Figure 13 shows the experimental (jagged) rate profiles (time vs Ri) at pH 6. The smooth lines were obtained using eq 2 with T_0 = 173.2 K, T_e = 228 K, T_a = 3002 K, and A = 99. The calculated T_a also changed from 2900 to 3200 K, as the SERS temperature increased from 1.5 to 55.3 °C, but this was within the range observed by Dubois (*10*).

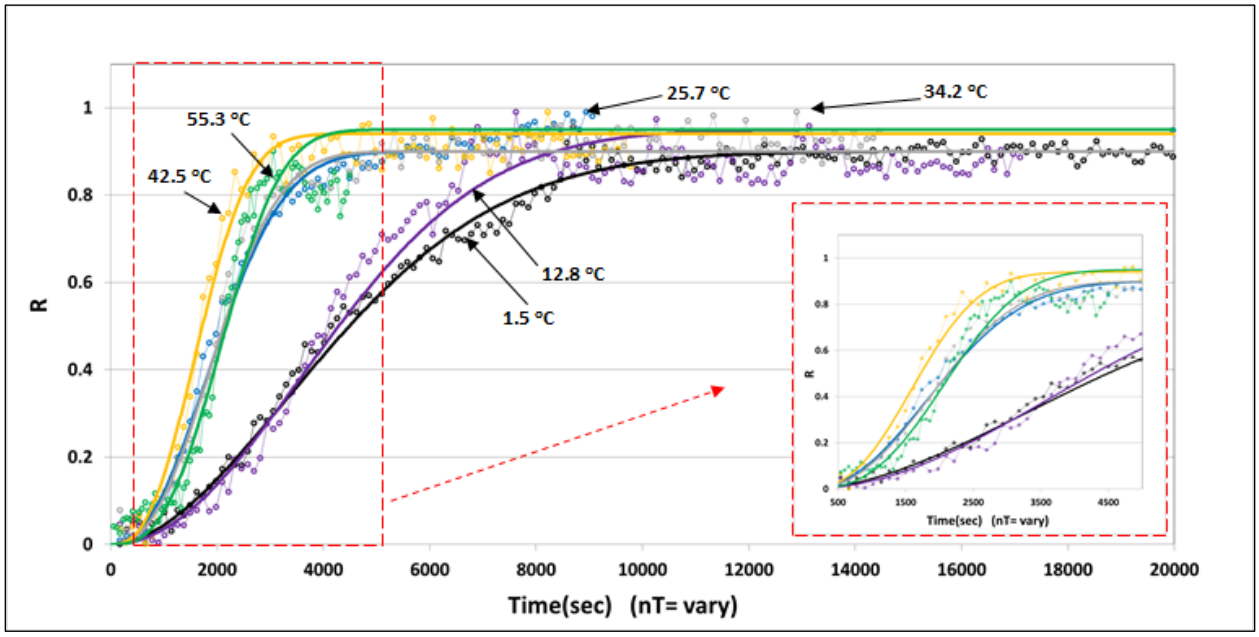

Figure 13. Experimental (jagged) rate profiles (time vs Ri) at pH 6. Smooth lines were obtained using eq 2 with T_a = 3002 K, T_0 = 173.2 K, T_e = 228 K, and A = 99.

Figure 14 shows experimental (jagged) rate profiles (time vs Ri) at pH 10. The smooth lines were obtained using eq 2 with T_0 = 184 K, T_e = 293 K, T_a = 3870 K, and A = 99. The calculated T_a also changed from 3500 to 4200 K, as the SERS temperature decreased from 53.7 to 1.7 °C, and it was 900 K higher than the range observed by Dubois et al. (*10*). This was expected because of the energy difference between chemisorption of thiophenol (acidic solution) and thiophenolate (base solution) to gold Klarite substrate.

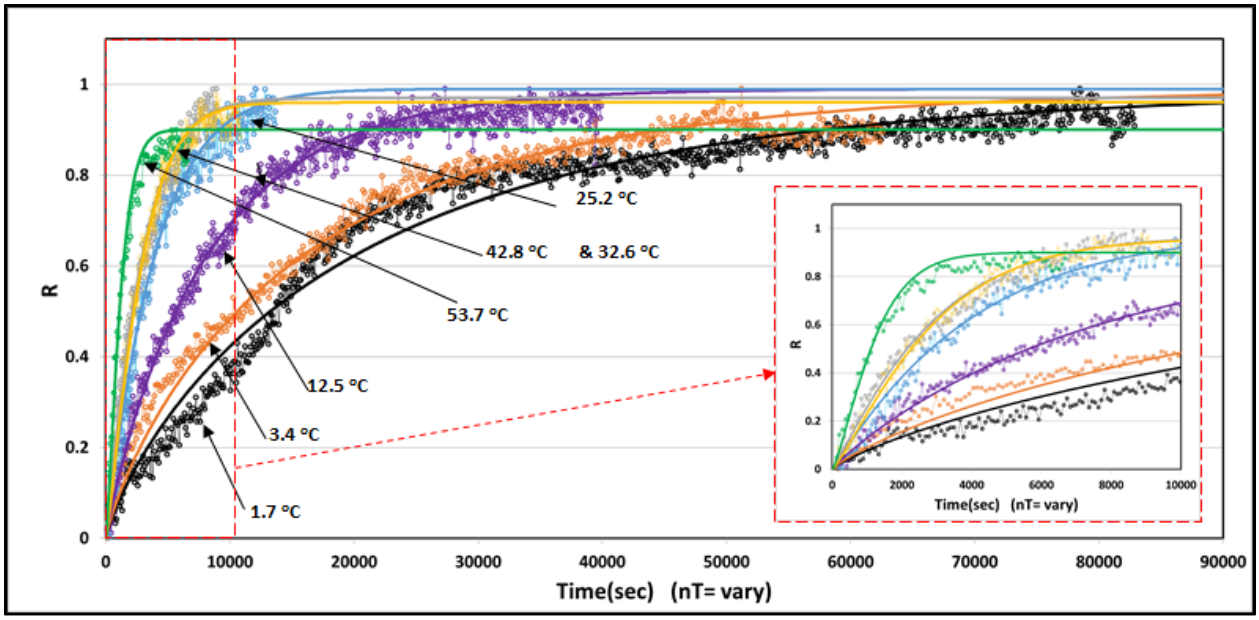

Figure 14. Experimental (jagged) rate profiles (time vs Ri) at pH 10. Smooth lines were obtained using eq 2 with T_a = 3870 K, T_0 = 184 K, T_e = 293 K, and A = 99.

Observations from Figures 11 to 14 can be summarized as follows:

1. The experimental (jagged) rate profiles show that an m-power value of t is temperature- and pH-dependent. Because m is a function of temperature and pH, the observed activation energy (E_{obs}) becomes equal to mE_a.
2. A reasonably linear relationship between m and temperature was found.
3. A linear relationship exists between T_e and pH.
4. A reasonably linear relationship exists between T_0 and pH.
5. The T_a value at pH < 7 was within the range obtained by other researchers (*10*). The T_a value at pH > 7 was higher by 900 K because of the elimination of one mechanism step.
6. Two activation energies were found, T_a = 3000 K at pH < 7 and T_a = 3900 K at pH > 7, which suggest two mechanisms. These two distinct adsorption regimes are dependent on the pH, which is experimentally centered about pH 6. At higher pH values, the activation energy (T_a = 3900 K) is 30% higher than that found at low pH values (T_a = 3000 K), which indicates a change in chemisorption as the rate-limiting step.
7. A single kinetic rate model was constructed from all 25 rate profiles without assumptions for any physicochemical rate mechanisms or without the influence of any rate model or default parameter.

4. CONCLUSIONS

A single kinetic rate model was constructed from experimental data without any assumptions or without the influence of any existing rate model. Studies reported herein have shown the robustness of the self-constructed kinetic rate model. The self-constructed kinetic rate equation includes temperature and pH as dependent variables. The calculated parameters (T_0, T_e, and T_a) elucidate the nature of the adsorption mechanisms of thiophenol on a Klarite gold substrate. The shifting mechanisms, due to the pH influence (protonated or deprotonated thiophenol), are explained in the calculated T_a values.

The mechanism of thiophenol binding onto a stationary gold substrate in aqueous media is shown to exhibit temperature- and pH-dependence. Although many studies have recognized the importance of pH in a SERS response, to our knowledge, this is the first study where rate profiles were generated at different temperature and pH values.

At low pH (e.g., pH 2.0), the thiophenol molecules are in a non-ionized form. At high pH (e.g., pH 10), the thiophenol molecules are in an ionized form (thiophenolate). The two forms have an impact on the adsorption activation energy.

The derived rate model, reported herein, showed that the thiophenol adsorption onto gold Klarite substrate was mainly chemisorption in nature at high pH values. At low pH values, thiophenol adsorption onto gold Klarite substrate was also chemisorption with an element of physisorption by the sulfhydryl hydrogen.

Experimental thiophenol adsorption rate profiles showed a variety of curve shapes from simple exponential (fast initial adsorption rate) to an S-shaped curve with an initially slow adsorption rate (delay). These variations can be modeled with a single rate equation.

Thiophenol adsorption has nearly a constant, relatively low T_a (3000 K) at pH 6 and below, but the T_a increased by 900 K (T_a = 3900 K at pH 10). The T_a at 3000 K is consistent with the Au–S adsorption bond. The increase in T_a by 900 K (3900–3000 K) was consistent with respect to the difference of the thiophenol and thiophenolate adsorption mechanisms due to pH or protonation.

Blank

LITERATURE CITED

1. Ho, Y.S.; McKay, G. Application of Kinetic Models to the Sorption of Copper(II) on to Peat. *Adsorp. Sci. Technol.* **2002,** *20* (8), 797–815.

2. Fleischman, M.; Hendra, P.J.; McQuillan, A.J. Raman Spectra of Pyridine Adsorbed at a Silver Electrode. *Chem. Phys. Lett.* **1974,** *26* (2), 163–166.

3. Le Ru, E.C.; Etchegoin, P.G. *Principles of Surface-Enhanced Raman Spectroscopy and Related Plasmonic Effects*; Elsevier: Amsterdam, 2009.

4. Seelenbinder, J.A.; Brown, C.W.; Urish, D.W. Self-Assembled Monolayers of Thiophenol on Gold as a Novel Substrate for Surface-Enhanced Infrared Absorption. *Appl. Spectrosc.* **2000,** *54* (3), 366–370.

5. Love, J.C.; Estroff, L.A.; Kriebel, J.K.; Nuzzo, R.G.; Whitesides, G.M. Self-Assembled Monolayers of Thiolates on Metals as a Form of Nanotechnology. *Chem. Rev.* **2005,** *105* (4), 1103−1169.

6. Schreiber, F. Structure and Growth of Self-Assembling Monolayers. *Prog. Surf. Sci.* **2000,** *65* (5−8), 151−256.

7. Schwartz, D.K. Mechanisms and Kinetics of Self-Assembled Monolayer Formation. *Annu. Rev. Phys. Chem.* **2001,** *52,* 107−137.

8. Nara, J.; Higai, S.; Morikawa, Y.; Ohno, T. Density Functional Theory Investigation of Benzenethiol, Adsorption on Au(111). *J. Chem. Phys.* **2004,** *120* (14), 6705−6711.

9. Dumee, L.; Hill, M.R.; Duke, M.; Velleman, L.; Sears, K.; Schultz, J.; Finn, N.; Gray, S. Activation of Gold Decorated Carbon Nanotube Hybrids for Targeted Gas Adsorption and Enhanced Catalytic Oxidation. *J. Mater. Chem.* **2012,** *22* (18), 9374–9378.

10. Dubois, L.H.; Zegarski, B.R.; Nuzzo, R.G. Molecular Ordering of Organosulfur Compounds on Au(111) and Au(100): Adsorption from Solution and in Ultrahigh Vacuum. *J. Chem. Phys.* **1993,** *98* (1), 678–688.

11. Li, S.J.; Wu, D.Y.; Xu, X.Y.; Gu, R.N. Theoretical and Experimental Studies on the Adsorption Behavior of Thiophenol on Gold Nanoparticles. *J. Raman Spectrosc.* **2007,** *38* (11), 1436–1443.

12. Nuzzo, R.G.; Zegarski, B.R.; Dubois, L.H. Fundamental Studies of the Chemisorption of Organosulfur Compounds on Gold (111). Implications for Molecular Self-Assembly on Gold Surfaces. *J. Am. Chem. Soc.* **1987,** *109* (3), 733–740.

13. Wetterer, S.M. Helium Atom Reflectivity Study of Physisorption and Chemisorption on Single Crystal Metal Surfaces; PhD Dissertation from Princeton University, Department of Chemistry, Princeton, NJ, November 1998, Chapter 4.

14. Biggs, K.B.; Camden, J.P.; Anker, J.N.; Van Duyne, R.P. Surface-Enhanced Raman Spectroscopy of Benzenethiol Adsorbed from the Gas Phase onto Silver Film over Nanosphere Surfaces: Determination of the Sticking Probability and Detection Limit Time. *J. Phys. Chem. A* **2009,** *113* (16), 4581−4586.

15. Carron, K.T.; Hurley, L.G. Axial and Azimuthal Angle Determination with Surface-Enhanced Raman-Spectroscopy – Thiophenol on Copper, Silver, and Gold Metal-Surfaces. *J. Phys. Chem.* **1991,** *95* (24), 9979−9984.

16. Christou, K.; Knorr, I.; Ihlemann, J.; Wackerbarth, H.; Beushausen, V. Fabrication and Characterization of Homogeneous Surface-Enhanced Raman Scattering Substrates by Single Pulse UV-Laser Treatment of Gold and Silver Films. *Langmuir* **2010,** *26* (23), 18564−18569.

17. Kang, H.; Park, T.; Choi, I.; Lee, Y.; Ito, E.; Hara, M.; Noh, J. Formation of Large Ordered Domains in Benzenethiol Self-Assembled Monolayers on Au(111) Observed by Scanning Tunneling Microscopy. *Ultramicroscopy* **2009,** *109* (8), 1011−1014.

18. Hill, W.; Wehling, B. Potential- and pH-dependent Surface-Enhanced Raman Scattering of *p*-Mercapto Aniline on Silver and Gold Substrates. *J. Phys. Chem.* **1993,** *97* (37), 9451−9455.

19. Lee, H.M.; Kim, M.S.; Kim, K. Surface-Enhanced Raman Scattering of *ortho*- and *para*-Mercaptophenols in Silver Sol. *Vib. Spectrosc.* **1994,** *6* (2), 205−214.

20. Kim, K.; Kim, K. L.; Shin, D.; Choi, J.-Y.; Shin, K.S. Surface-Enhanced Raman Scattering of 4-Aminobenzenethiol on Ag and Au: pH Dependence of b_2-Type Bands. *J. Phys. Chem. C* **2012,** *116* (7), 4774−4779.

21. Li, S.J.; Wu, D.Y.; Xu, X.Y.; Gu, R.N. Theoretical and Experimental Studies on the Adsorption Behavior of Thiophenol on Gold Nanoparticles. *J. Raman Spectrosc.* **2007,** *38* (11), 1436−1443.

22. Tripathi, A.; Emmons, E.D.; Christesen, S.D.; Fountain, A.W., III; Guicheteau, J.A. Kinetics and Reaction Mechanisms of Thiophenol Adsorption on Gold Studied by Surface-Enhanced Raman Spectroscopy. *J. Phys. Chem. C* **2013,** *117* (44), 22834−22842.

23. Tripathi, A.; Emmons, E.D.; Fountain, A.W., III; Guicheteau, J.A.; Moskovits, M.; Christesen, S.D. Critical Role of Adsorption Equilibria on the Determination of Surface-Enhanced Raman Enhancement. *ACS Nano.* **2015,** *9* (1), 584−93.

24. Candlin, J.P.; Wilkins, R.G. Sulphur-Nitrogen Compounds. Part I. The Hydrolysis of Sulphamate Ion in Perchloric Acid. *J. Chem. Soc.* **1960,** 4236−4241.

25. Danehy, J.P.; Noel, C.J. The Relative Nucleophilic Character of Several Mercaptans toward Ethylene Oxide. *J. Am. Chem. Soc.* **1960,** *82* (10), 2511−2515.

26. Pascal, I.; Tarbell, D.S. The Kinetics of the Oxidation of a Mercaptan to the Corresponding Disulfide by Aqueous Hydrogen Peroxide. *J. Am. Chem. Soc.* **1957,** *79* (22), 6015−6020.

27. Altarawneh, M.; Dar, T.; Dlugogorski, B.Z. Thermochemical Parameters and pK_a Values for Chlorinated Congeners of Thiophenol. *J. Chem. Eng. Data* **2012,** *57* (6), 1834−1842.

28. Maswadeh, W.; Vanderbeek, R.; Emmons, E.; Guicheteau, J.; Tripathi, A. *Universal Rate Model Selector: A Method to Quickly Find the Best-Fit Kinetic Rate Model for an Experimental Rate Profile*; ECBC-TR-1477; U.S. Army Edgewood Chemical Biological Center: Aberdeen Proving Ground, MD, 2017; UNCLASSIFIED Report.

29. *The Chemistry of the Thiol Group*; Patai, S., Ed.; Chemistry of Functional Groups, Part 2; John Wiley and Sons: London, 1974; pp 721–735.

30. Lanin, S.N.; Pichugina, D.A.; Shestakov, A.F.; Smirnova, V.V.; Nikolaev, S.A.; Lanina, K.S.; Vasil'kov, A.Y.; Zung, F.T.; Beletskaya, A.V. Hydrocarbon Adsorption on Gold Clusters: Experiment and Quantum Chemical Modeling. *Russ. J. Phys. Chem. A* **2010,** *84* (12), 2133–2142.

31. Holze, R. The Adsorption of Thiophenol on Gold – A Spectroelectrochemical Study. *Phys. Chem. Chem. Phys.* **2015,** *17* (33), 21364–21372.

32. Aider, M.; Arul, J.; Mateescu, M.A.; Brunet, S.; Bazinet, L. Electromigration Behavior of a Mixture of Chitosan Oligomers at Different Concentrations. *J. Agric. Food Chem.* **2006,** *54* (26), 10170−10176.

33. Sánchez-Moreno, P.; Ortega-Vinuesa, J.L.; Martín-Rodríguez, A.; Boulaiz, H.; Marchal-Corrales, J.A.; Peula-García, J.M. Characterization of Different Functionalized Lipidic Nanocapsules As Potential Drug Carriers. *Int. J. Mol. Sci.* **2012,** *13* (2), 2405−2424.

34. Light, T.S. Temperature Dependence and Measurement of Resistivity of Pure Water. *Anal. Chem.* **1984,** *56* (7), 1138−1142.

Blank

ACRONYMS AND ABBREVIATIONS

3D	three-dimensional
A	Arrhenius constant
ASC	analyte sample chamber
E_a	activation energy
E_{obs}	observed activation energy
Exo-Rx	exothermic reaction
I	SERS intensity
I_{max}	experimental maximum SERS intensity
I_{min}	experimental minimum SERS intensity
m	ratio equal to $(1 - T/T_0)/(1 - T/T_e)$
PBE	Perdew, Burke, and Ernzerhow function
pK_a	acid dissociation constant
R	universal gas constant
Ri	relative intensity
Ri_{max}	a fitting parameter from 0.90 to 1.0 (if the collected data did not reach saturation or equilibrium)
SCRM	self-constructing rate modeling
SEM	scanning electron microscopy
SERS	surface-enhanced Raman spectroscopy
T	temperature
t	time
T_0	temperature of immobility of analyte
T_a	temperature of activation
TC–ASC	temperature-controlled–analyte sample chamber system
T_e	temperature of the system at equilibrium and pH = 0
T_{freeze}	temperature where ions and molecules are frozen or immobilized
$T_{immobilization}$	temperature where ions and molecules are immobilized
$TP_{–S^-}$	ionized thiophenolate
$TP_{–S–H}$	non-ionized thiophenol molecules
T_{room}	room temperature
T_{water}	water temperature

DISTRIBUTION LIST

The following individuals and organizations were provided with one Adobe portable document format (pdf) electronic version of this report:

U.S. Army Combat Capabilities
Development Command
Chemical Biological Center
(CCDC CBC)
Spectroscopy Branch
FCDD- CBR-IS
ATTN: Maswadeh, W.
Vanderbeek, R.
Emmons, E.
Guicheteau, J.
Tripathi, A.

CCDC CBC
Technical Library
FCDD-CBR-L
ATTN: Foppiano, S.
Stein, J.

Defense Threat Reduction Agency
DTRA-RD-IAR
ATTN: Pate, B.

Defense Technical Information Center
ATTN: DTIC OA

U.S. ARMY COMBAT CAPABILITIES DEVELOPMENT COMMAND
CHEMICAL BIOLOGICAL CENTER